7446 *Inorg. Chem.* **2009**, *48*, 7446–7451
DOI: 10.1021/ic901067z

Inorganic Chemistry
Article

Effect of an In-Plane Ligand on the Electronic Structures of Bromo-Bridged Nano-Wire Ni−Pd Mixed-Metal Complexes, $[Ni_{1-x}Pd_x(bn)_2Br]Br_2$ (bn = 2*S*,3*S*-Diaminobutane)

Mari Sasaki,[†] Hashen Wu,[†] Daisuke Kawakami,[†] Shinya Takaishi,[†] Takashi Kajiwara,[†] Hitoshi Miyasaka,[†] Brian K. Breedlove,[†] Masahiro Yamashita,*[,†] Hideo Kishida,[§] Hiroyuki Matsuzaki,[‡] Hiroshi Okamoto,[‡] Hisaaki Tanaka,[§] and Shinichi Kuroda[§]

[†]*Graduate School of Science, Tohoku University, Aramaki-Aza-Aoba, Aoba-Ku, Sendai 980-8578, Japan,* [‡]*Graduate School of Frontier Science, The University of Tokyo & CREST (JST), 5-1-5 Kashiwanoha, Kashiwa, Chiba 277-8561, Japan, and* [§]*Graduate School of Engineering, Nagoya University, Furo-Cho, Chikusa-Ku, Nagoya 464-8603, Japan*

Received June 3, 2009

Single crystals of quasi-one-dimensional bromo-bridged Ni−Pd mixed-metal complexes with 2*S*,3*S*-diaminobutane (bn) as an in-plane ligand, $[Ni_{1-x}Pd_x(bn)_2Br]Br_2$, were obtained by using an electrochemical oxidation method involving mixed methanol/2-propanol (1:1) solutions containing different ratios of $[Ni^{II}(bn)_2]Br_2$ and $[Pd^{II}(bn)_2]Br_2$. To investigate the competition between the electron-correlation of the Ni^{III} states, or Mott-Hubbard states (MH), and the electron−phonon interaction of the $Pd^{II}-Pd^{IV}$ mixed valence states, or charge-density-wave states (CDW), in the Ni−Pd mixed-metal compounds, X-ray structure analyses, X-ray oscillation photograph, and Raman, IR, ESR, and single-crystal reflectance spectra were analyzed. In addition, the local electronic structures of Ni−Pd mixed-metal single crystals were directly investigated by using scanning tunneling microscopy (STM) at room temperature and ambient pressure. The oxidation states of $[Ni_{1-x}Pd_x(bn)_2Br]Br_2$ changed from a $M^{II}-M^{IV}$ mixed valence state to a M^{III} MH state at a critical mixing ratio (x_c) of ∼0.8, which is lower than that of $[Ni_{1-x}Pd_x(chxn)_2Br]Br_2$ (chxn=1*R*,2*R*-diaminocyclohexane) ($x_c \approx 0.9$) reported previously. The lower value of x_c for $[Ni_{1-x}Pd_x(bn)_2Br]Br_2$ can be explained by the difference in their CDW dimensionalities because the three-dimensional CDW ordering in $[Pd(bn)_2Br]Br_2$ observed by using X-ray diffuse scattering stabilizes the $Pd^{II}-Pd^{IV}$ mixed valence state more than two-dimensional CDW ordering in $[Pd(chxn)_2Br]Br_2$ does, which has been reported previously.

Introduction

Recently, low-dimensional compounds have been attracting much attention since they show very interesting physical properties, such as Peierls transition, spin-Peierls transition, neutral-ionic transitions, charge-density wave states (CDWs), spin-density wave states (SDWs), and superconductivity, because of crystal structures with low dimensionalities and electronic structures.[1] In short, the interactions between the spin, charge, phonon, and electron in low-dimensional systems produce interesting physical phenomena. Among such low-dimensional compounds, quasi-one-dimensional halogen-bridged mixed valence Pt, Pd, and Ni compounds (hereafter abbreviated as MX-Chains) have been extensively investigated over the last 30 years because of their very unique and interesting physical properties, such as intense and dichroic intervalence charge transfer bands, luminescence with large Stokes shifts, progressive overtones in the resonance Raman spectra, midgap absorptions attributable to solitons and polarons, large third-order non-linear optical properties, non-linear electrical conductivities, field effect transistor (FET) performances, one-dimensional (1D) model compounds of high T_c copper-oxide superconductors, and so forth.[2] Moreover, these compounds show the largest

*To whom correspondence should be addressed. E-mail: yamasita@agnus.chem.tohoku.ac.jp.

(1) (a) Miller, J. S. *Extended linear chain compounds*; Plenum Press: New York, 1982; Vol. *1*−*3*. (b) Andrieux, A.; Jerome, D.; Bechgaard, K. *J. Phys., Lett.* **1981**, *42*, 87–90. (c) Su, W. P.; Schrieffer, J. R.; Heeger, A. J. *Phys. Rev. B* **1980**, *22*, 2099–2111.

(2) (a) Clark, R. J. H. *Adv. Infrared Raman Spectrosc.* **1983**, *11*, 95–130. (b) Clark, R. J. H.; Franks, M. L.; Trumble, W. R. *Chem. Phys. Lett.* **1976**, *41*, 287–292. (c) Clark, R. J. H.; Kurmoo, M.; Mountney, D. N.; Toftland, H. *J. Chem. Soc., Dalton Trans.* **1982**, *1982*, 1951–1860. (d) Tanino, H.; Kobayashi, K. *J. Phys. Soc. Jpn.* **1983**, *52*, 1446–1256. (e) Tanaka, M.; Kurita, S.; Kojima, T.; Yamada, Y. *Chem. Phys.* **1984**, *91*, 257–265. (f) Iwasa, Y.; Funatsu, E.; Hasegawa, T.; Koda, T.; Yamashita, M. *Appl. Phys. Lett.* **1991**, *59*, 2219–2221. (g) Wada, Y.; Mitani, T.; Yamashita, M.; Koda, T. *J. Phys. Soc. Jpn.* **1985**, *54*, 3143–3153. (h) Okamoto, H.; Yamashita, M. *Bull. Chem. Soc. Jpn.* **1998**, *71*, 2023–2039. (i) Takaishi, S.; Yamashita, M. *Chem. Lett.* **2008**, *37*, 382–387. (j) Takaishi, S.; Yamashita, M.; Matsuzaki, H.; Okamoto, H.; Tanaka, H.; Kuroda, S.; Goto, A.; Shimizu, T.; Takenobu, T.; Iwasa, Y. *Chem.—Eur. J.* **2008**, *14*, 472–477. (k) Clark, R. J. H. *Chem. Soc. Rev.* **1984**, *13*, 219–244. (l) Clark, R. J. H. *Chem. Soc. Rev.* **1990**, *19*, 107–131. (m) Toriumi, K.; Okamoto, H.; Mitani, T.; Bandow, S.; Yamashita, M.; Wada, Y.; Fujii, Y.; Clark, R. J. H.; Michael, D. J.; Edward, A. J.; Watkin, D.; Kurmoo, M.; Day, P. *Mol. Cryst. Liq. Cryst.* **1990**, *181*, 333–342.

 Published on Web 07/08/2009

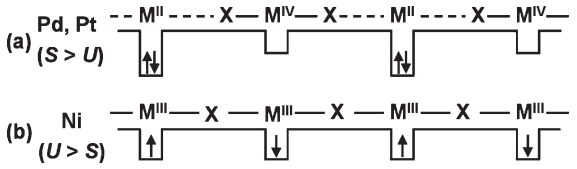

Figure 1. Diagrams of the structures of M(II)−M(IV) mixed valence compounds of (a) Pt and Pd, and (b) Ni(III) Mott−Hubbard states.

third-order optical non-linearity[3] and very fast response or relaxation (<1 ps) from photoexcited states.[4] Therefore, these compounds are very promising for use in optical switches, optical communications, and optical computers.

From a theoretical viewpoint, these compounds are classified as Peierls-Hubbard systems, where the electron−phonon interaction (S), the electron transfer energy (T), the on-site and intersite Coulomb repulsion energies (U and V, respectively) compete or cooperate with each other.[5] The Pt and Pd compounds form CDW or M(II)−M(IV) mixed valence states (Figure 1a), where the bridging halogens are displaced from the midpoints between two neighboring metal ions because of S. Thus, the half-filled metallic bands are split into occupied valence bands composed of M(II) d_{z^2} orbitals and unoccupied conduction bands composed of M(IV) d_{z^2} orbitals with finite Peierls energy gaps. Therefore, they are class II type compounds of the Robin−Day classification for mixed valence complexes,[6] except for one example reported recently.[7] These compounds are formulated as $[M^{II}(AA)_2][M^{IV}X_2(AA)_2]Y_4$ (M^{II},M^{IV} = Pt^{II},Pt^{IV}, Pd^{II},Pd^{IV}, Pd^{II},Pt^{IV}, Ni^{II},Pt^{IV}, and Cu^{II},Pt^{IV}: X = Cl, Br, I, and mixed halides; AA = ethylenediamine (en), diaminocyclohexane (chxn), etc.; Y = ClO_4, BF_4, X, etc.). On the other hand, the Ni compounds form Ni^{III}−Ni^{III} MH states (Figure 1b), where the bridging halogens are located at the midpoints between two neighboring Ni ions because of a strong U.[8] Therefore, these Ni complexes are class III type compounds of the Robin-Day classification for mixed valence complexes.[6] The half-filled Ni(III) d_{z^2} bands are split into upper-Hubbard bands (UHBs) and lower-Hubbard bands (LHBs) because of a strong U. The energy levels of the bridging halogen are located between the UHBs and the LHBs. Therefore, strictly speaking, the Ni(III) compounds are regarded as not Mott−Hubbard (MH) insulators but as charge transfer (CT) insulators. Strong antiferromagnetic interactions between the spins located on the Ni(III) d_{z^2} orbitals through the bridging halogens have been observed in these Ni complexes ($J \approx -2800$ cm^{-1}) because of strong p-d hybridization. Among various nanowire materials, such as polyacetylene (a type of Peierls insulator) and polysilane (a type of band insulator), investigated so far,[3] $[Ni(chxn)_2Br]Br_2$ shows the largest third-order optical nonlinearity ($\sim 10^{-4}$ esu) because of strong quantum confinement effect.

Recently, a series of single crystals of quasi-1D bromo-bridged Ni and Pd mixed-metal complexes, $[Ni_{1-x}Pd_x(chxn)_2Br]Br_2$, have been synthesized by using electrochemical methods.[9] The electronic structures of these complexes have been extensively studied by means of X-ray diffuse scattering, IR, resonance Raman, and single-crystal reflectance spectroscopies, magnetic susceptibilities, and scanning tunneling microscopy (STM).[10] It has been found that oxidation states of $[Ni_{1-x}Pd_x(chxn)_2Br]Br_2$ change at a critical amount of Pd ions (x_c) of $\sim$0.9 (x_c is the critical value). In other words, these compounds are in a +3 MH state when $x_c < 0.9$ and a Pd^{II}−Pd^{IV} mixed valence state when $x_c > 0.9$. On the other hand, on the basis of X-ray diffuse scattering studies, $[Pd(bn)_2Br]Br_2$ showed three-dimensional CDW ordering, whereas $[Pd(chxn)_2Br]Br_2$ shows two-dimensional CDW ordering, as previously reported. Therefore, the difference in their CDW dimensionalities, as well as the difference in the size of the ligands, should influence the electronic structures of $[Ni_{1-x}Pd_x(AA)_2Br]Br_2$ (AA = chxn and bn). Thus, to investigate the effect of the in-plane ligands and dimensionalities of CDW on the electronic structures of $[Ni_{1-x}Pd_x(AA)_2Br]Br_2$, we analyzed IR, ESR, and single-crystal reflectance spectra, as well as STM images of $[Ni_{1-x}Pd_x(bn)_2Br]Br_2$.

Experimental Section

The starting compounds $[Ni(bn)_2]Br_2$ and $[Pd(bn)_2]Br_2$ were synthesized by using methods similar to those for $[Ni(chxn)_2]Br_2$ and $[Pd(chxn)_2]Br_2$, respectively.[9] The Ni−Pd mixed-metal compounds, $[Ni_{1-x}Pd_x(bn)_2Br]Br_2$, were synthesized by using methods similar to those for $[Ni_{1-x}Pd_x(chxn)_2Br]Br_2$.[9] The ratios of Ni and Pd ions were determined by using ICP emission measurements on a Shimadzu ICPS 7510 plasma spectrometer. Single crystals of $[Pd(bn)_2Br]Br_2$ were obtained by using electrochemical oxidation methods in a 1:1 (v/v) solution of methanol/2-propanol containing $[Pd(bn)_2]Br_2$ and tetramethylammonium bromide. Anal. Calcd for $C_8H_{24}N_4PdBr_3$: C, 18.39; H, 4.63; N, 10.72. Found: C, 18.31; H, 4.44; N, 10.74.

Single crystal X-ray structure determination was carried out on a Bruker SMART CCD diffractometer using graphite-monochromated Mo Kα ($\lambda = 0.7107$ Å). An X-ray oscillation photograph was acquired on a MacScience Imaging Plate diffractometer using a synchrotron generated X-ray source installed in beamline 1B at the photon factory of the High Energy Accelerator Research Organization (KEK-PF). ESR spectra were measured on a Bruker EMX spectrometer equipped with a gas-flow type cryostat (Oxford ESR 900). Polarized reflectivity spectra were obtained by

(3) Kishida, H.; Matsuzaki, H.; Okamoto, H.; Manabe, T.; Yamashita, M.; Taguchi, Y.; Tokura, Y. *Nature* **2000**, *405*, 929–932.
(4) (a) Matsuzaki, H.; Yamashita, M.; Okamoto, H. *J. Phys. Soc. Jpn.* **2006**, *75*, 123701-1. (b) Tao, S.; Miyagoe, T.; Maeda, A.; Matsuzaki, H.; Ohtsu, H.; Kasegawa, M.; Takaishi, S.; Yamashita, M.; Okamoto, H. *Adv. Mater.* **2007**, *19*, 2707–2710.
(5) (a) Baeriswyl, D.; Bishop, A. R. *J. Phys. C* **1988**, *21*, 339–356. (b) Mishima, A.; Nasu, K. *Phys. Rev. B* **1989**, *40*, 5593–5597.
(6) Robin, M. B.; Day, P. *Adv. Inorg. Radiochem.* **1967**, *10*, 247–422.
(7) Takaishi, S.; Takamura, M.; Kajiwara, T.; Miyasaka, H.; Yamashita, M.; Iwata, M.; Matsuzaki, H.; Okamoto, H.; Tanaka, H.; Kuroda, S.; Nishikawa, H.; Oshio, H.; Takata, M. *J. Am. Chem. Soc.* **2008**, *130*, 12080–12084.
(8) (a) Toriumi, K.; Wada, Y.; Mitani, T.; Bandow, S.; Yamashita, M.; Fujii, Y. *J. Am. Chem. Soc.* **1989**, *111*, 2341–2342. (b) Okamoto, H.; Toriumi, K.; Mitani, T.; Yamashita, M. *Phys. Rev. B* **1990**, *42*, 10381–10387. (c) Okamoto, H.; Shimada, Y.; Oka, Y.; Chainani, A.; Takahashi, T.; Kitagawa, H.; Mitani, T.; Toriumi, K.; Inoue, K.; Manabe, T.; Yamashita, M. *Phys. Rev. B* **1996**, *54*, 8438–8445.
(9) (a) Yamashita, M.; Ishii, T.; Matsuzaka, H.; Manabe, T.; Kawashima, T.; Okamoto, H.; Kitagawa, H.; Mitani, T.; Marumoto, K.; Kuroda, S. *Inorg. Chem.* **1999**, *38*, 5124–5130. (b) Marumoto, K.; Kuroda, S.; Manabe, T.; Yamashita, M. *Phys. Rev. B* **1999**, *60*, 7699–7720. (c) Tanaka, H.; Marumoto, K.; Kuroda, S.; Manabe, T.; Yamashita, M. *J. Phys. Soc. Jpn.* **2002**, *71*, 1370–1375. (d) Matsuzaki, H.; Iwano, K.; Aizawa, T.; Ono, M.; Kishida, H.; Yamashita, M.; Okamoto, H. *Phys. Rev. B* **2004**, *70*, 035204-1–035204-7.
(10) Takaishi, S.; Miyasaka, H.; Sugiura, K.; Yamashita, M.; Matsuzaki, H.; Kishida, H.; Okamoto, H.; Tanaka, H.; Marumoto, K.; Ito, H.; Kuroda, S.; Takami, T. *Angew. Chem., Int. Ed.* **2004**, *43*, 3171–3175.

using a specially designed spectrometer with a 25 cm grating monochromator and an optical microscope. Optical conductivity spectra were obtained by performing a Kramers–Kronig transformation on the reflectivity spectra. Raman spectra were measured on a Renishaw Raman spectrometer. STM measurements were performed at room temperature and ambient pressure. Single-crystals were cleaved and mounted on a sample stage with carbon paste so that the surface of the *bc* plane could be observed. All STM images were acquired in a constant height mode on a JEOL JSPM-5200 microscope. A positive sample bias voltage (V_g) was used.

Results and Discussion

1. Crystal Structure and Electronic State of $[Pd(bn)_2Br]Br_2$. Figure 2a shows a crystal structure of $[Pd(bn)_2Br]Br_2$. The space group of $[Pd(chxn)_2Br]Br_2$ is *I*222 (orthorhombic),[11] whereas that of $[Pd(bn)_2Br]Br_2$ is *C*2 (monoclinic), which is same as that of $[Ni(bn)_2Br]Br_2$, because of the lower repulsion between the bn ligands of neighboring chains, as observed in Figure 2b. Two bn ligands coordinate to Pd ions in the equatorial plane, and two Br^- ions coordinate to Pd ions in the axial positions, forming linear −Pd−Br−Pd−Br− chain structures. Two-dimensional hydrogen-bond networks between the amino protons of the bn ligands and Br^- ions were observed along the chains and between the chains, which are similar to that of $[Ni(bn)_2Br]Br_2$. The Pd···Pd distance along the chain of this compound is slightly shorter than that of $[Pd(chxn)_2Br]Br_2$. The most important point is the position of the bridging Br^- ions along the chain. In $[Pd(chxn)_2Br]Br_2$, the bridging Br^- ions are displaced from the midpoints between two neighboring Pd ions, causing two different Pd−Br distances (2.516 Å for Pd(IV)−Br and 2.777 Å for Pd(II)···Br). Therefore, this $[Pd(chxn)_2Br]Br_2$ compound is in a Pd(II)−Pd(IV) mixed valence state, and its formula is correctly written as $[Pd^{II}(chxn)_2][Pd^{IV}(chxn)_2Br_2]Br_4$. On the other hand, the bridging Br^- ions in $[Pd(bn)_2Br]Br_2$ are located near the midpoints between neighboring Pd ions without disorder. However, there are two possibilities to describe the state of this molecule: one is a real Pd(III) MH state, and the other is a Pd(II)−Pd(IV) mixed valence state, where the positions of the bridging Br^- ions cannot be separated because of a tiny displacement of the bridging Br^- ions. Although it is impossible to determine the oxidation states of the Pd ions by using single-crystal X-ray structure analysis in this case, scanning tunneling microscopy (STM) can be used because electronic structure can be observed directly via tunnel currents. An STM image of $[Pd(bn)_2Br]Br_2$ in the *bc* plane with dimensions of 200 × 200 Å is shown in Figure 3a. Bright spots are observed every 10×7 Å. The Pd−Pd distance along the *b* (1D chain) and *c* axes are 5.26 and 7.05 Å, respectively. These spots in the image reflect the 2-fold periodicity of the valence structure that results from the CDW structure of $[Pd(bn)_2Br]Br_2$. Therefore, strictly speaking, $[Pd(bn)_2Br]Br_2$ should be formulated as $[Pd^{II}(bn)_2][Pd^{IV}(bn)_2Br_2]Br_4$. The Pd(II)−Pd(IV) mixed valence state in this compound was also determined on the basis of the IR and ESR spectra, as discussed later.

(11) Hazell, A. *Acta Crystallogr.* **1991**, *C47*, 962–966.

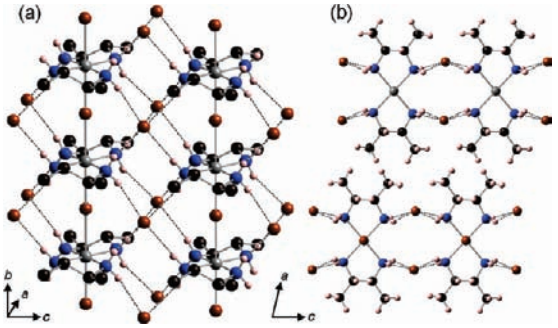

Figure 2. Crystal structure of $[Pd(bn)_2Br]Br_2$ projected on the (a) *a* axis and (b) *b* axis. Gray: Pd; Brown: Br; Black: C; Blue: N; Pink: H. Hydrogen atoms bonding to the carbon atoms are omitted for clarity for (a).

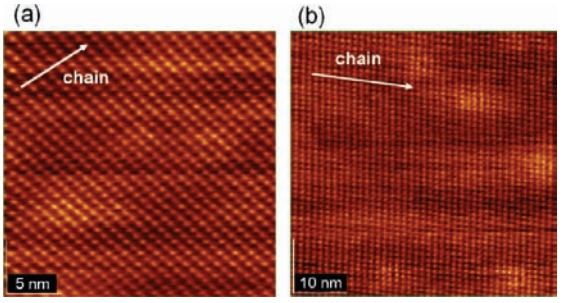

Figure 3. STM images of $[Pd(bn)_2Br]Br_2$ with dimensions of (a) 200 × 200 Å and (b) 500 × 500 Å.

Figure 3b shows an STM image of this compound with dimensions of 500×500 Å. The bright spots were aligned without any phase mismatches within the measured area, indicating that the CDW phase is completely aligned in the *bc* plane. This situation is in contrast to that of $[Pd(chxn)_2Br]Br_2$, which shows short-range ordering of the CDW phase along the *c*-axis. X-ray oscillation photography is also a useful way to determine the dimensionalities of the CDW state. Such investigations have been carried out extensively, and as a result, it has been shown that the CDW dimensionalities strongly depend on the type of counteranions. For example, 1D CDW ordering is observed when ClO_4^- is the counterion, whereas short-range two-dimensional CDW ordering is observed when halogen counterions, such as Cl^-, Br^-, and I^-, are used.[12] This difference is due to hydrogen-bonding. The compounds with ClO_4^- counterions have a 1D hydrogen bond network along the chains, whereas the compounds with X^- counterions have two-dimensional hydrogen-bond networks along the chains and between the chains. X-ray oscillation photographs with rotation along the chain were acquired for $[Pd(bn)_2Br]Br_2$, as shown in Figure 4. Superlattice reflections were observed as clear spots, rather than diffuse spots, indicating that $[Pd(bn)_2Br]Br_2$ has three-dimensional CDW ordering. This three-dimensional CDW ordering in $[Pd(bn)_2Br]Br_2$ should stabilize the Pd(II)−Pd(IV) mixed valence state more than that in $[Pd(chxn)_2Br]Br_2$ because of the higher dimensionality of the CDW ordering. This is consistent with the results obtained from the STM images of these compounds.

(12) Yamashita, M.; Manabe, T.; Kawashima, T.; Shimizu, H. *Trends Chem. Phys.* **1999**, *7*, 1–33.

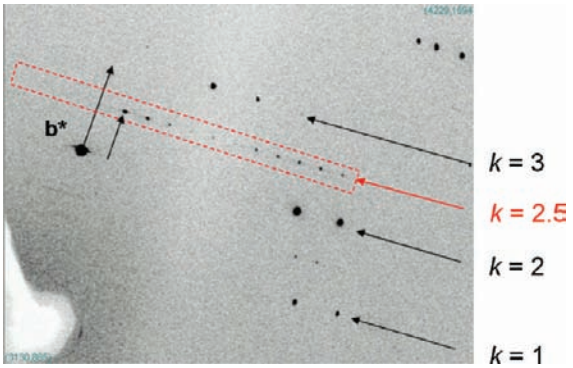

Figure 4. X-ray oscillation photograph of $[Pd(bn)_2Br]Br_2$.

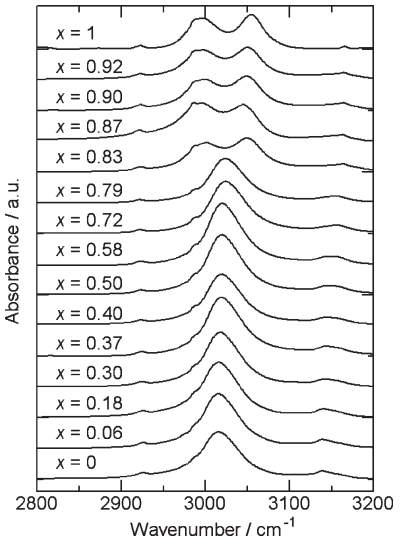

Figure 5. IR spectra of $[Ni_{1-x}Pd_x(bn)_2Br]Br_2$.

2. Electronic Structures of $[Ni_{1-x}Pd_x(bn)_2Br]Br_2$. The peaks for the N−H stretching modes, which are observed around 3000 cm^{-1} in the IR spectra, are very good probes for evaluating electronic states. Ni(III) compounds show a single peak for the N−H stretching mode because there is only one oxidation state (i.e., all Ni(III) ions), whereas Pd(II)−Pd(IV) mixed valence compounds show two peaks for the N−H stretching modes because of the two oxidation states.[13] As shown in Figure. 5, two peaks for the N−H stretching modes were observed when x_c exceeded about 0.8, whereas those for the chxn compounds are observed when x_c exceeds ~0.9.[9d] As described in the above section, the $[Pd(bn)_2Br]Br_2$ shows three-dimensional CDW ordering, whereas $[Pd(chxn)_2Br]Br_2$ shows two-dimensional CDW ordering. Therefore, the Pd(II)−Pd(IV) mixed valence states of $[Pd(bn)_2Br]Br_2$ should be more stable than those of $[Pd(chxn)_2Br]Br_2$, resulting in the lower value of x_c (~0.8) for $[Ni_{1-x}Pd_x(bn)_2Br]Br_2$ compared with that (~0.9) for $[Ni_{1-x}Pd_x(chxn)_2Br]Br_2$.

The spin susceptibilities of these compounds should reflect the oxidation states. Figure 6 shows the magnitudes of the spin susceptibilities of $[Ni_{1-x}Pd_x(bn)_2Br]Br_2$ along with $[Ni_{1-x}Pd_x(chxn)_2Br]Br_2$. If spinless Pd ions (Pd(II) or Pd(IV)) are incorporated into the 1D antiferromagnetic (AF) chain, the AF chain is disrupted, affording many non-interacting spins at the end of odd-numbered chain fragments, which generate a large magnetic moment. In this case, the spin susceptibility should increase with x. In the present compounds, however, the spin susceptibilities remained almost constant in the range of $0 < x < x_c$, indicating that Pd(III) ions with a spin of 1/2 are incorporated into the 1D AF chain such that they do not disrupt it. For $x > x_c$, the Pd(III) ions gradually convert to non-magnetic Pd(II)−Pd(IV) mixed valence states, as observed in the IR spectra described in the previous paragraph. In Figure 6, the fluctuating behavior was barely observed in the range of $x < x_c$. Such behavior may be due to the difference in the J values of the AF interactions between the Ni(III) and Pd(III) ions.

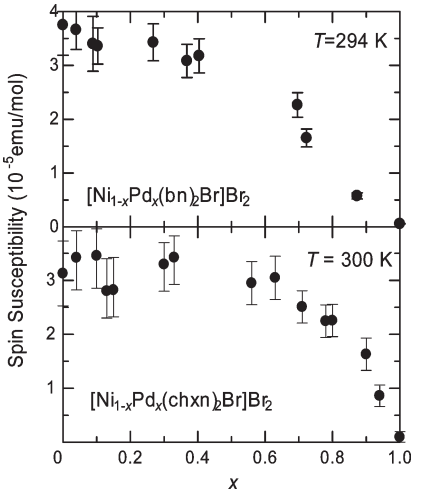

Figure 6. Spin susceptibilities of $[Ni_{1-x}Pd_x(bn)_2Br]Br_2$ and $[Ni_{1-x}Pd_x(chxn)_2Br]Br_2$.

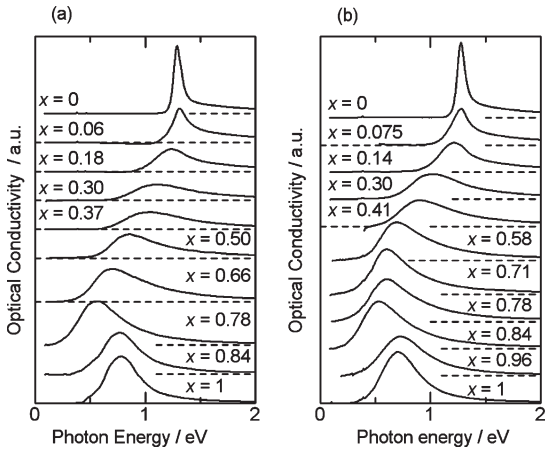

Figure 7. Optical conductivity spectra of (a) $[Ni_{1-x}Pd_x(bn)_2Br]Br_2$ and (b) $[Ni_{1-x}Pd_x(chxn)_2Br]Br_2$.

Optical conductivity spectra of $[Ni_{1-x}Pd_x(bn)_2Br]Br_2$ together with those of $[Ni_{1-x}Pd_x(chxn)_2Br]Br_2$ are shown in Figure 7. The pure Ni(III) compound $[Ni(bn)_2Br]Br_2$ ($x = 0$) exhibited a prominent sharp peak at around 1.3 eV. This peak was attributed to a CT transition from the bridging Br p_z orbital to a Ni UHB, as shown in Figure 8a. In the range of $0.18 < x < 0.78$, the peak shifted to lower energy with an increase in x. This situation is

(13) Okaniwa, K.; Okamoto, H.; Mitani, T.; Toriumi, K.; Yamashita, M. *J. Phys. Soc. Jpn.* **1991**, *60*, 997–1004.

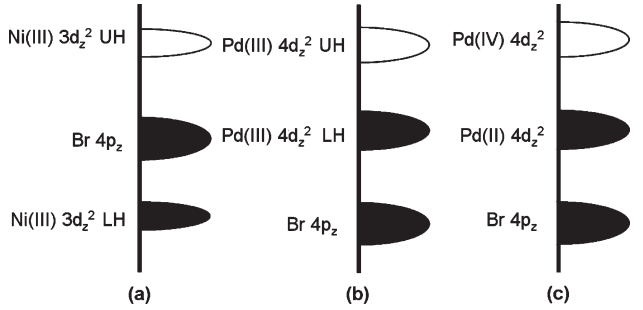

Figure 8. Electronic structures and CT bands of (a) Ni(III) CT insulator, (b) Pd(III) Mott−Hubbard insulator, and (c) Pd(II)−Pd(IV) CDW state.

similar to that of $[Ni_{1-x}Pd_x(chxn)_2Br]Br_2$. In this range, the peak was attributed to a transition from a Pd(III) LHB to a Pd(III) UHB, as shown in Figure 8b. In addition, there was a discontinuous change in energy in the range of $0.78 < x < 0.84$. The energy of the peak for $x = 0.84$ is almost equal to that of the peak for the pure Pd compound $[Pd(bn)_2][Pd(bn)_2Br_2]Br_4$ ($x = 1$), which has been attributed to an intervalence charge transfer (IVCT) transition from an occupied Pd(II) d_{z^2} orbital to an unoccupied Pd(IV) d_{z^2} orbital, as shown in Figure. 8c. Thus, on the basis of the optical conductivity spectra, the critical value for the conversion from the Pd(II)−Pd(IV) mixed valence states to the Pd(III) MH states (x_c) of $[Ni_{1-x}Pd_x(bn)_2Br]Br_2$ was determined to be ~0.8, whereas that of $[Ni_{1-x}Pd_x(chxn)_2Br]Br_2$ is ~0.9. These results are reasonably consistent with those from the analyses of the IR and ESR spectra.

To investigate the local electronic structures of $[Ni_{1-x}Pd_x(bn)_2Br]Br_2$, we analyzed STM images of single-crystals at room temperature and ambient pressure. Figure 9a shows an STM image of $[Ni(bn)_2Br]Br_2$ with dimensions of 200×200 Å. Bright spots were observed in the image every 5×7 Å. The crystal structure of $[Ni(bn)_2Br]Br_2$ is shown in Figure. 9b. The Ni···Ni distances along the *b* axis (1D chain) and *c* axes are 5.13 and 7.10 Å, respectively, meaning these spots reflect the periodicity of $[Ni(bn)_2]$ units in the *bc* plane. In other words, all of the Ni centers are equivalent and in a +3 oxidation state in $[Ni(bn)_2Br]Br_2$. This finding is consistent with the results obtained from single-crystal X-ray analysis. As the STM measurements were performed with positive sample bias, the tunnel current is from the Fermi energy (E_F) of the tip to a conduction band of the sample. Therefore, in case of $[Ni(chxn)_2Br]Br_2$, the tunnel current is from E_F to the d_{z^2} UHBs of Ni(III) ions.

Next, we carried out STM measurements on the Ni−Pd mixed-metal compounds $[Ni_{1-x}Pd_x(bn)_2Br]Br_2$. Figure 10 shows STM images of the compounds with $x =$ (a) 0.46, (b) 0.69, (c) 0.72, and (d) 0.83 and dimensions of 200×200 Å. For the compound with $x = 0.46$ (Figure 10a), an image similar to that of $[Ni(bn)_2Br]Br_2$ was obtained; that is, almost no 2-fold periodicity was observed. This result shows that the compound with $x = 0.46$ contains mostly Ni(III) and Pd(III) oxidation states. In the image of the compound with $x = 0.69$ (Figure 10b), on the other hand, 2-fold periodicity was observed in patches, which we attributed to Pd(II)−Pd(IV) CDW states. In Figure 10c where $x = 0.72$, the CDW coherence was

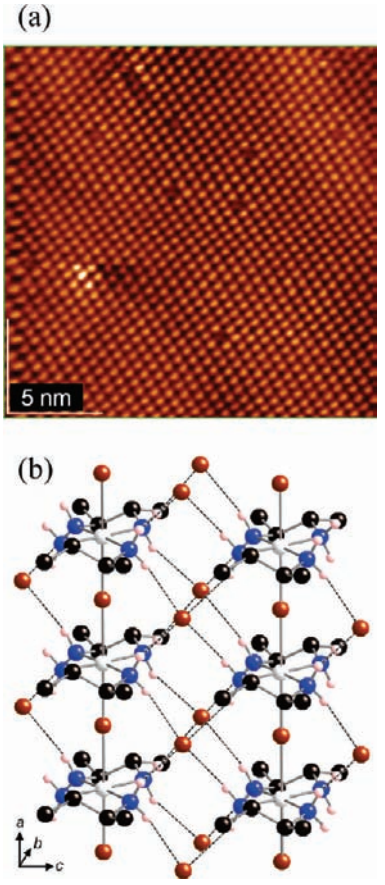

Figure 9. (a) STM image and (b) crystal structure of $[Ni(bn)_2Br]Br_2$. White: Ni, Brown: Br, Black: C, Blue: N, Pink: H. Hydrogen atoms bonding to the carbon atoms are omitted for clarity.

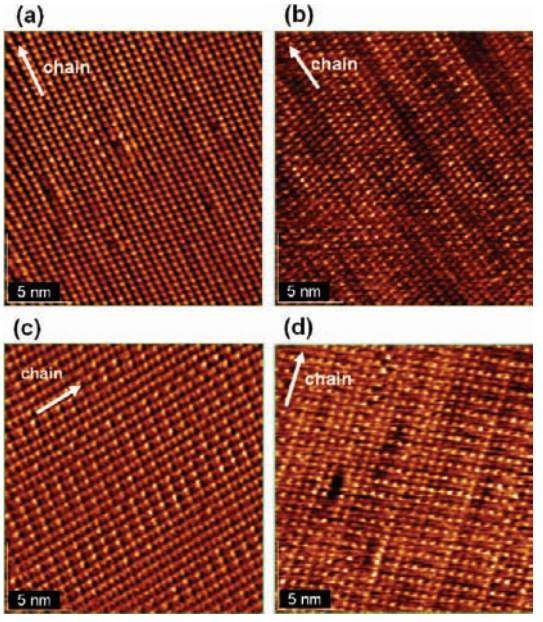

Figure 10. STM images of $[Ni_{1-x}Pd_x(bn)_2Br]Br_2$ with $x =$ (a) 0.46, (b) 0.69, (c) 0.72, and (d) 0.83 on the *bc* plane (200 × 200 Å).

spread over approximately 30 metal sites along the *b* axis and 4 or 5 metal sites along the *c* axis. Figure 10d shows an STM image of the compound with $x = 0.83$. A large part of this image showed 2-fold periodicity; that is, a

Pd(II)−Pd(IV) CDW state was observed. For the bn complexes, the value of x_c was 0.8, at which the oxidation states of the Pd ions changed from Pd(III) MH states to Pd(II)−Pd(IV) mixed valence states. In the case of the chxn complexes, the value of x_c has been reported to be 0.9. The values were determined on the bases of IR, ESR, and reflectance spectra, and the difference was determined to be due to the CDW dimensionalities and the bulkiness of the ligands.

Conclusion

$[Pd(bn)_2][Pd(bn)_2Br_2]Br_4$ exhibited three-dimensional CDW ordering, whereas $[Pd(chxn)_2][Pd(chxn)_2Br_2]Br_4$ exhibits two-dimensional CDW ordering. The three-dimensional ordering causes the Pd(II)−Pd(IV) CDW states in $[Pd(bn)_2][Pd(bn)_2Br_2]Br_4$ to be more stable than those in $[Pd(chxn)_2][Pd(chxn)_2Br_2]Br_4$. We investigated the effects of the bn and chxn ligands on the electronic structures of $[Ni_{1-x}Pd_x(AA)_2Br]Br_2$ (AA = bn and chxn), in which the electron−phonon interaction (S) and electron-correlation (U) compete with each other. As a result, in the case of the Ni−Pd mixed-metal compounds $[Ni_{1-x}Pd_x(bn)_2Br]Br_2$, the critical amount of Pd ions (x_c) where the Pd(II)−Pd(IV) CDW states convert to Pd(III) MH states was determined to be ∼0.8 on the basis of IR and ESR spectroscopies, single-crystal optical conductivity, and STM measurements, whereas in case of $[Ni_{1-x}Pd_x(chxn)_2Br]Br_2$, it has been reported to be ∼0.9. We concluded that the different values of x_c were due to the difference in the CDW dimensionalities and the bulkiness of the ligands.

Acknowledgment. The authors wish to acknowledge Dr. Y. Wakabayashi at KEK for the X-ray diffusion measurements. This work was partly supported by a Grant-in-Aid for Creative Scientific Research from the Ministry of Education, Culture, Sports, Science, and Technology of Japan.

Supporting Information Available: X-ray crystallographic information of compound $[Pd(bn)_2Br]Br_2$ in CIF format. This material is available free of charge via the Internet at http://pubs.acs.org.